Pressure Distribution and Global Forces on a Bridge Deck Section: Experimental and CFD Analysis of Static Aerodynamic Forces

D. Rocchi[1]; T. Argentini[2]; and M. Sbrosi[3]

Introduction

Three different approaches can be adopted for the evaluation of the aerodynamic forces of bridge decks: measurement of global forces, measurement of pressure distribution, and computational fluid dynamics (CFD) analysis. Each of these approaches has its benefits and drawbacks. On the one hand, if experimental methods are considered, the knowledge of pressure distributions is important to understand the underlying physics of the fluid-structure interaction, but it is not applicable to estimate global force coefficients if traffic barriers, railings, or wind shields are present. In this case, the only practicable way is to measure global forces with dynamometric models. On the other hand, CFD simulations are not reliable unless they are validated against experimental data and are therefore used as a complementary tool to assess the experimental results and eventually to perform some numerical aerodynamic tailoring before a final check in the wind tunnel.

In light of these considerations, the present research aims to compare the first two approaches for the evaluation of the static (stationary) aerodynamic forces on a simple deck section without barriers. Experimental aerodynamic forces are measured in wind tunnels both by using a dynamometric balance and by integrating the pressure distribution along the contour of the deck section; the results are then compared. A CFD analysis is then used as a complementary tool to analyze the differences between the two experimental measurement systems.

[1]Researcher, Dept. of Mechanical Engineering, Politecnico di Milano, via La Masa 1, 20156 Milano, Italy. E-mail: daniele.rocchi@polimi.it

[2]Researcher, Dept. of Mechanical Engineering, Politecnico di Milano, via La Masa 1, 20156 Milano, Italy (corresponding author). E-mail: tommaso.argentini@polimi.it

[3]Ph.D. Candidate, Dept. of Mechanical Engineering, Politecnico di Milano, via La Masa 1, 20156 Milano, Italy. E-mail: marco.sbrosi@mail.polimi.it

Note. This manuscript was submitted on February 17, 2014; approved on August 18, 2014; published online on September 16, 2014. Discussion period open until February 16, 2015; separate discussions must be submitted

Concerning CFD, several authors reported that, for bridge decks, three-dimensional (3D) models considering detached eddy simulations (DES) or large eddy simulations (LES) provide more accurate results than two-dimensional (2D) Reynolds-averaged Navier-Stokes (RANS) simulations (Watanabe and Fumoto 2008; Watanabe et al. 2004; Bai et al. 2010; Sarwar et al. 2008; Mannini et al. 2010). In this study, however, a 2D RANS approach is adopted for its low computational cost, with the objective of using the numerical results as a tool for the evaluation of the measurement errors induced by both tap discretization and the lack of shear-stress effects. In the numerical analysis, several turbulence models for the RANS equations are analyzed. The deck section aerodynamics are investigated comparing the modification of the pressure distribution and the corresponding global forces at different angles of attack. Different considerations can be done for different angles of attack because of the different flow field structure around the section and in particular because of the presence of flow separation and the effects of shear stresses.

Ricciardelli and Hangan (2001) compared experimental pressure distributions and aerodynamic forces on a different simplified deck section and found some discrepancies between the results of the two measurement methods. The larger differences concern the drag coefficient, but these discrepancies are not deeply investigated because the aim of their paper was not the comparison of the two different measurement approaches. In this study, using a different simplified deck section specifically chosen for this purpose, similar discrepancies are obtained and discussed, with the support of experimental and numerical results.

The results presented in this paper, focused on the evaluation of stationary aerodynamic forces, are part of a larger research project aimed at validating the postprocess of the dynamometric measurements during forced and free-motion tests (Diana et al. 2004). In particular, it is important to assess the dynamic performances of the dynamometric measurement systems to correctly measure self-excited nonstationary forces during aeroelastic tests on suspended section models. Such tests are necessary to validate 2D aerodynamic force models, especially when aerodynamic nonlinearities are investigated (Diana et al. 2013, 2008, 2010). In fact, direct dynamometric

force measurements give the sum of the aerodynamic and inertial contribution as a result, whereas a pressure system only allows the measurement of aerodynamic effects. In stationary conditions the inertial effects are not present, and the direct dynamometric measurement is taken as a reference to investigate the critical aspects of distributed pressure measurements. The analysis of experimental aerodynamic forces in nonstationary aeroelastic conditions has been presented in Argentini et al. (2012), and a CFD investigation will be presented in a future paper.

This paper is structured as follows. The characteristics of the experimental setup are summarized, with a specific focus on the force measurement devices, pointing out the assumptions and the hypothesis adopted. Then, a critical analysis of the experimental results is presented, highlighting the differences that emerged from the two different measurement systems. Discrepancies between the results are then investigated by means of a 2D CFD RANS analysis using a commercial code. The CFD results and model settings are described: geometry, mesh, boundary conditions, and turbulence models. Numerical results are used to assess experimental results. Finally, conclusions and final remarks are presented.

Wind Tunnel Tests

Wind tunnel tests were performed at the Wind Tunnel of Politecnico di Milano. A single-box deck section with a simple shape was chosen to perform the desired tests. The deck shape is taken from an actual highway bridge, neglecting the traffic barriers on the upper surface (Fig. 1). This simplification allows the measurement of the aerodynamic forces directly through the integration of the pressure distribution (Ricciardelli and Hangan 2001), considering the contribution of shear stresses as negligible. The deck section model is 2.91 m long and 1 m wide. The geometry and main dimensions are reported in Fig. 1. The wind tunnel blockage is less than 1%, whereas the residual turbulence intensities in the vertical and horizontal directions are, respectively, $I_w = 1.1\%$ and $I_u = 1.6\%$, with integral length scales ${}^xL_w = 0.025$ m and ${}^xL_u = 0.124$ m.

The dynamometric measurement system is mounted in the central part of the sectional model (0.91 m long) and consists of a set of seven load cells that are able to measure the force and moment components (Diana et al. 2004). The pressure measurement system consists of a ring of 78 pressure taps placed around the middle section of the model (Fig. 2), which are connected to high-frequency pressure scanners, allowing for a sampling frequency of 100 Hz. Sixteen additional pressure taps are distributed along four lines (correlation lines) aligned with the deck axis (see open diamonds in Fig. 2). To measure the pressure correlation in the axial direction, two are in the upper part and two are in the lower part. The distribution of the pressure taps was studied to refine the measurement where a strong pressure gradient was expected. Pressure measurements are performed simultaneously with the global force measurements obtained by internal balance.

The incoming wind is measured one chord upwind from the leading edge by means of a four-hole probe that resolves the instantaneous vertical and horizontal wind components. A photograph of the experimental setup is given in Fig. 3.

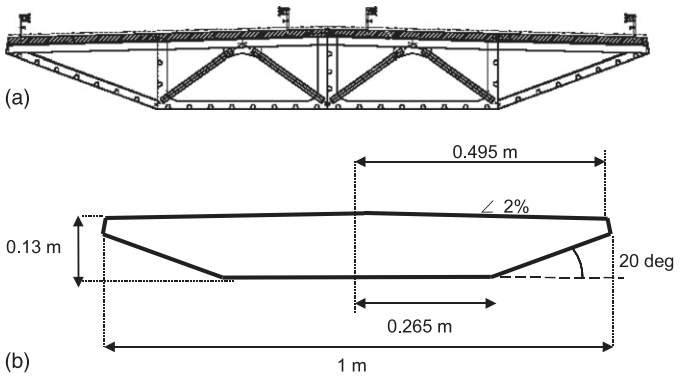

Fig. 1. Deck section dimensions and shape: (a) actual deck section with traffic barriers; (b) simplified deck section model, 1:30 scale

Experimental Aerodynamic Coefficients and Pressure Distributions

Static aerodynamic drag, lift, and pitching moment coefficients are expressed as

$$C_D(\theta) = \frac{D(\theta)}{\frac{1}{2}\rho U^2 B}; \quad C_L(\theta) = \frac{L(\theta)}{\frac{1}{2}\rho U^2 B}; \quad C_M(\theta) = \frac{M(\theta)}{\frac{1}{2}\rho U^2 B^2} \quad (1)$$

where ρ = air density; U = mean wind horizontal velocity; B = deck chord; D, L, and M = mean lift force, drag force, and pitching moment per unit length, respectively; and θ = angle of attack. Sign conventions for forces and pitch rotation are shown in Fig. 4.

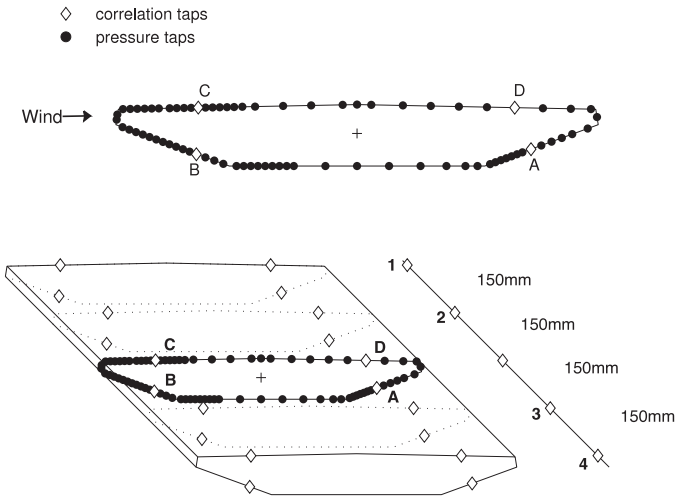

Fig. 2. Position of pressure taps and correlation lines

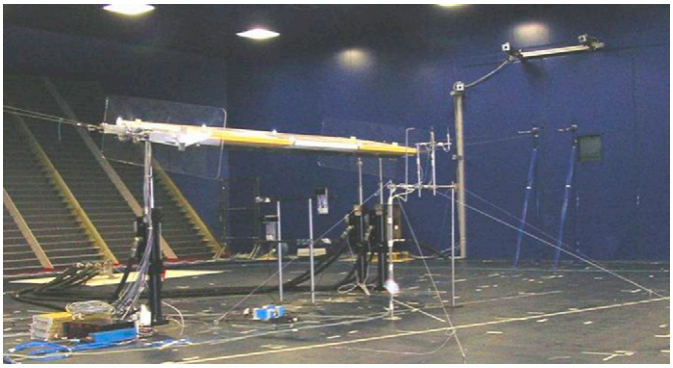

Fig. 3. Experimental setup during wind tunnel tests

Aerodynamic forces D, L, and M are obtained either from the measurement of the load cells or from the integration of the pressure distribution, assigning a tributary area to each pressure tap. In general, Reynolds number dependence should be considered (Hui et al. 2008). In the following, the Reynolds number is kept constant at 7×10^5 ($\mathrm{R} = UB/\nu$, $U = 10$ m/s).

Fig. 5 shows the aerodynamic coefficients as a function of the angle of attack. The following considerations can be done: the drag coefficient is underestimated by the pressure integration for negative angles of attack; or the lift and moment coefficients show a good agreement, but a slightly different slope of the coefficients is noticed. The lift coefficient from the pressure integration has a smaller slope, whereas the moment coefficient has a larger slope. These results are coherent with those found by Ricciardelli and Hangan (2001) for the Sunshine Skyway Bridge deck section.

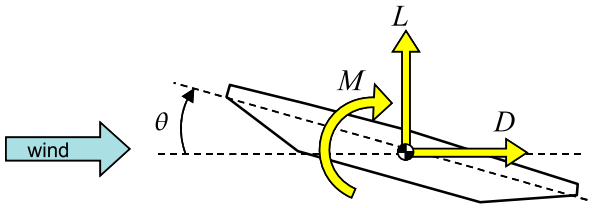

Fig. 4. Aerodynamic force conventions

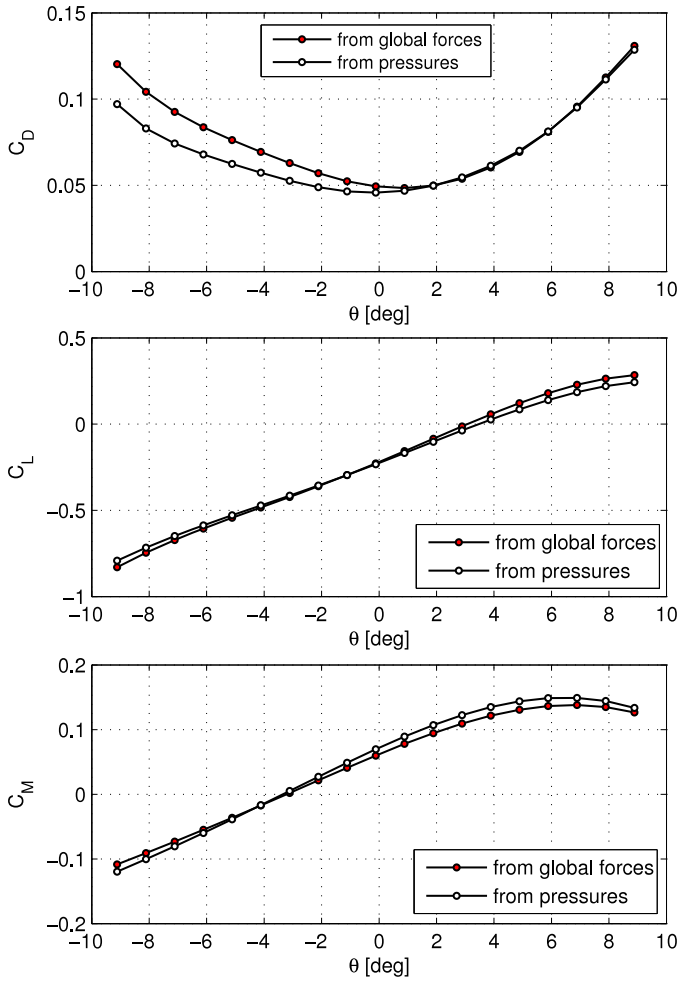

Fig. 5. Comparisons of aerodynamic coefficients versus θ

Comments about these results need a more accurate understanding of the flow-structure interaction mechanism. The knowledge of pressure distributions as a function of the angle of attack, shown in Figs. 6 and 7, provides a basis for this analysis. Pressure coefficients, C_p, defined as $p/(1/2\rho U^2)$, are shown as arrows normal to the deck surface that are pointing outward if pressure p is negative (suction); however, they point inward if p is positive.

For an angle of attack of $-9°$, the values of the pressure coefficients on the upper surface are low and positive toward the leading edge, which is an indication of no-flow separation around the upwind upper corner. In the lower surface, there is a complete separation, with negative pressure coefficients with high gradients, especially in the leading edge portion.

Increasing the angle of attack at -6 and $-3°$, there is an increasing small separation in the upper surface of the leading edge with negative pressures, followed by a smooth reattachment with very low pressure values. The lower surface is still in suction, with pressure coefficients that are smaller in the leading edge portion and nearly unchanged elsewhere.

For positive angles of attack, from 0 and 6°, there is an increasing portion of the upper surface, which is in suction, with a flow reattachment that increasingly moves toward the trailing edge. The lower part of the leading edge experiences an initial positive pressure region followed by a separation that anticipates the surface edge. At 9° there is a full separation, with negative constant pressure coefficients in the upper surface, whereas the separation in the lower part of the leading edge occurs near to the lower surface edge.

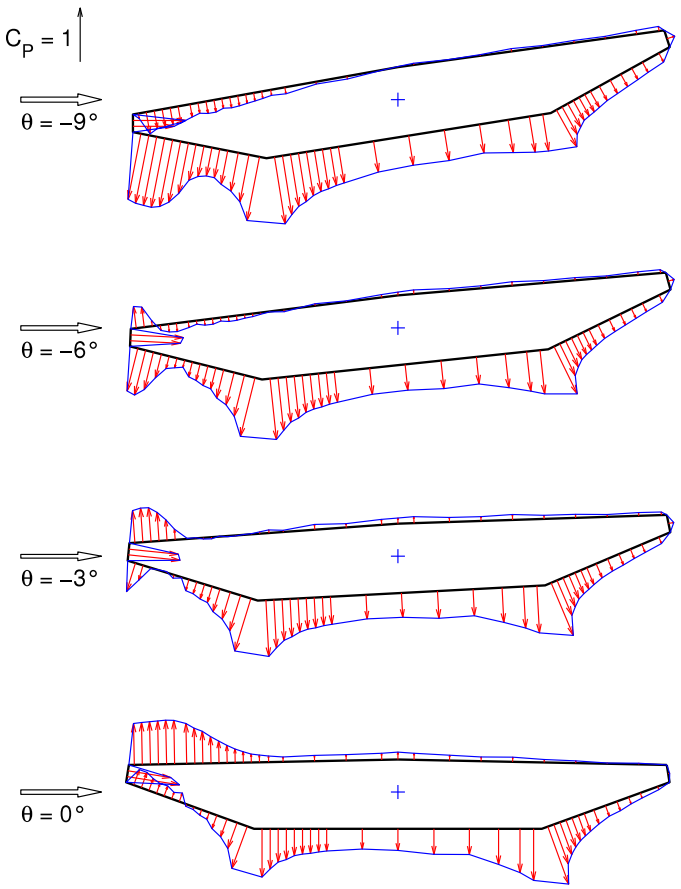

Fig. 6. Pressure coefficient distributions for negative angles of attack

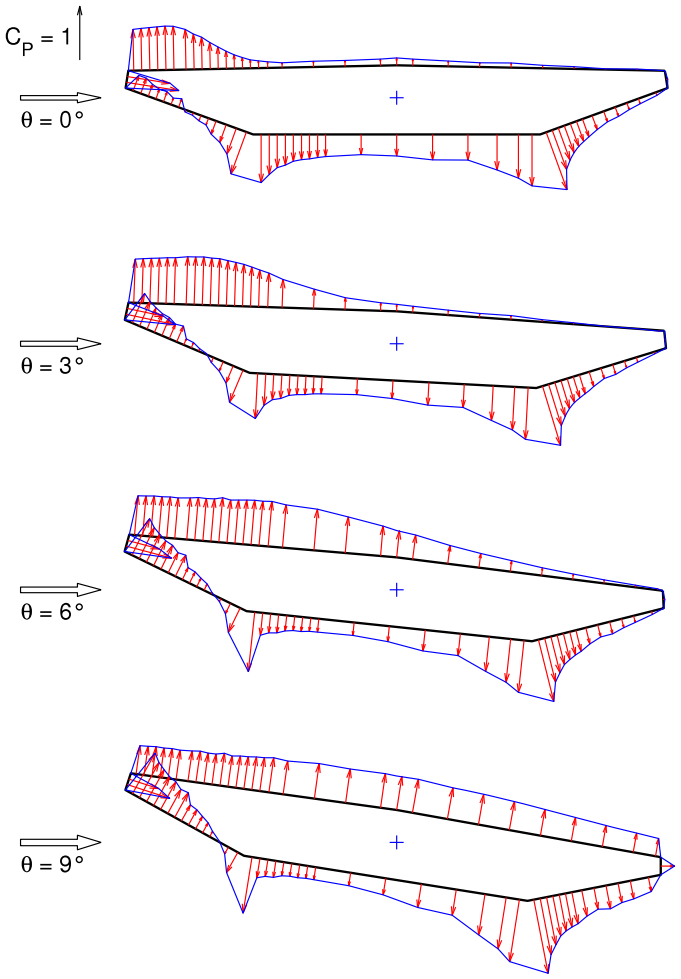

Fig. 7. Pressure coefficient distributions for positive angles of attack

In comparing the pressure distributions around the deck section for different angles of attack, the following considerations about the global coefficients may be drawn. The lift force is caused by the balance between the pressure on the upper and lower surfaces of the deck. The coefficient C_L is negative up to 3° where the separation bubble on the upwind upper region counterbalances the negative pressure produced on the lower surfaces by the flow acceleration.

The moment coefficient is negative up to −3°. At −9° there are two negative contributions to the pitching moment caused by the positive pressure on the upwind upper region and the negative pressure on the lower surfaces, which are mainly present in the upwind part. Moving toward the positive angles of attack, a negative pressure zone appears and expands in the upwind upper surface and a positive pressure field appears in the lower upwind region. The stagnation zone moves along the tilted surface for increasing angles of attack giving a positive contribution to the aerodynamic moment.

The discrepancies between the results of the two different measurement systems might be ascribed to the effect of

- Axial correlation (bidimensionality);
- Shear stresses; or
- Measurement grid discretization.

The bidimensionality of the flow field can be assessed by comparing the experimental mean pressure values along the correlation lines. Fig. 8 shows the spanwise mean pressure along the four axial lines (A, B, C, and D in Fig. 2), with respect to the central taps that are used for the integration of the pressure field. The diagrams also show the accuracy band of the pressure scanners (±2 Pa). In general, the pressure values are consistent, with some higher differences at specific locations/angles of attack.

These experimental comparisons can be used to estimate a correction of the pressure field nearby the correlation taps. For shear-stress and measurement grid discretization effects, a numerical analysis has been conducted to evaluate their influence through the definition of a discretization error and a shear-stress error.

CFD Analysis

The numerical analysis is focused on an investigation of experimental results to evaluate the discrepancies in the experimental mean aerodynamic coefficients between force and pressure systems. In particular, CFD are used to define the discretization error and shear-stress error.

The 2D steady-state flow simulations have been performed to compute the mean pressure distribution and mean aerodynamic forces because no significant unsteady phenomena and small separated flow regions are present in the experimental data. Steady-state RANS simulations are considered a good compromise between the achievable quality of the results and the computational effort for the analyzed problem; however, their shortcomings are well known.

Different turbulence models have been tested and compared in terms of accuracy and effectiveness in reproducing the experimental results, especially with regard to their capability of reproducing the separated flow regions. The solution of the fluid dynamic equations allows the separation of the effect of pressure and the shear contribution acting on the bridge surfaces. The resulting forces on the bridge deck are then computed by integrating the pressure and friction components along the boundary on the deck surfaces. Numerical results are compared with experimental measurements in terms of the pressure distribution around the deck profile and global force coefficients. The numerical solutions are carried out using *FLUENT 6.3* CFD code.

Fluid Domain, Geometry, and Boundary Conditions

The computational domain considered for CFD simulation reproduces the geometry of the bridge deck section in model scale and the wind tunnel test room. The dimensions of the fluid domain are shown in Fig. 9. The domain has been generated considering six deck chords before and 12 deck chords after the bridge deck section, respectively, to ensure independence from the boundary inlet condition and to allow for the development of the turbulent wake.

To perform a significant comparison between the numerical and experimental results, boundary conditions are set to reproduce the wind tunnel setup. The boundary conditions for the fluid domain are shown in Fig. 9. The fluid domain is surrounded by boundaries Γ^{up}, Γ^{down}, Γ^{in}, and Γ^{out}. The boundary conditions are applied on the domain boundaries as specified.

- Γ^{up} and Γ^{down}: the symmetry condition is used instead of the wall no-slip condition because no significant differences on the aerodynamic forces are shown between these two conditions. On the other hand, the symmetry condition allows for the reduction of the number of cells in the entire domain.
- Γ^{in}: the uniform inlet-velocity profile, normal to the boundary, has a magnitude of 10 m/s and 2% turbulence intensity as measured in wind tunnel tests.
- Γ^{out}: the zero-pressure outlet condition is used. (Note that this condition is legitimate only if the outlet boundary is far enough from the bridge trailing edge.)

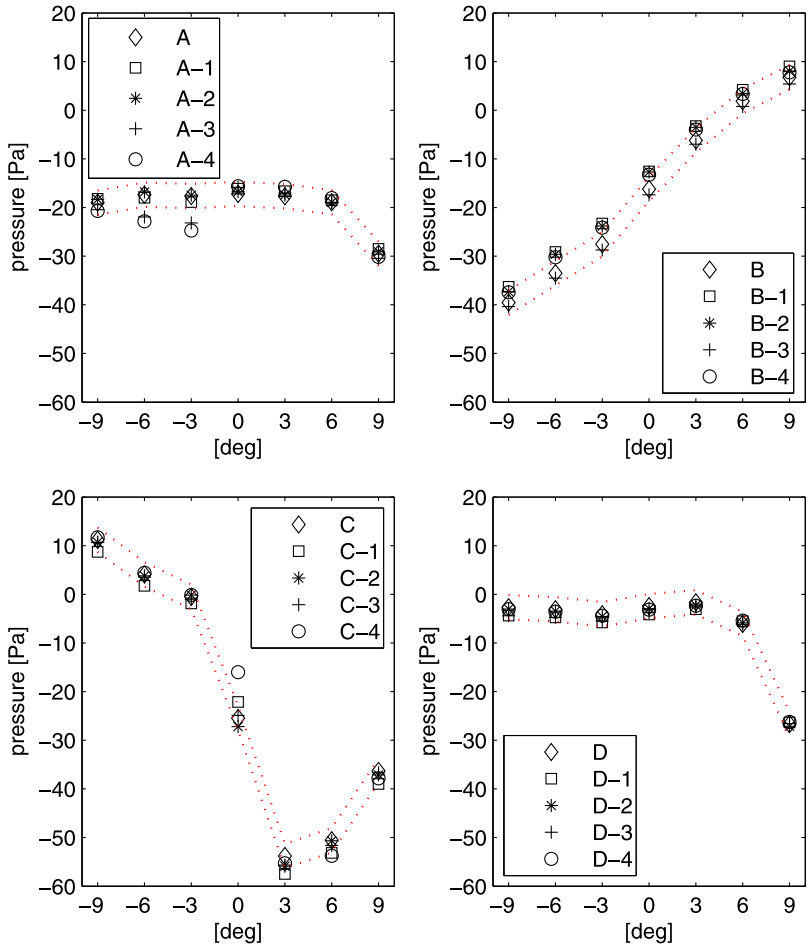

Fig. 8. Spanwise mean pressure versus static angle of attack; dotted lines represent the accuracy band of the pressure scanner (±2 Pa)

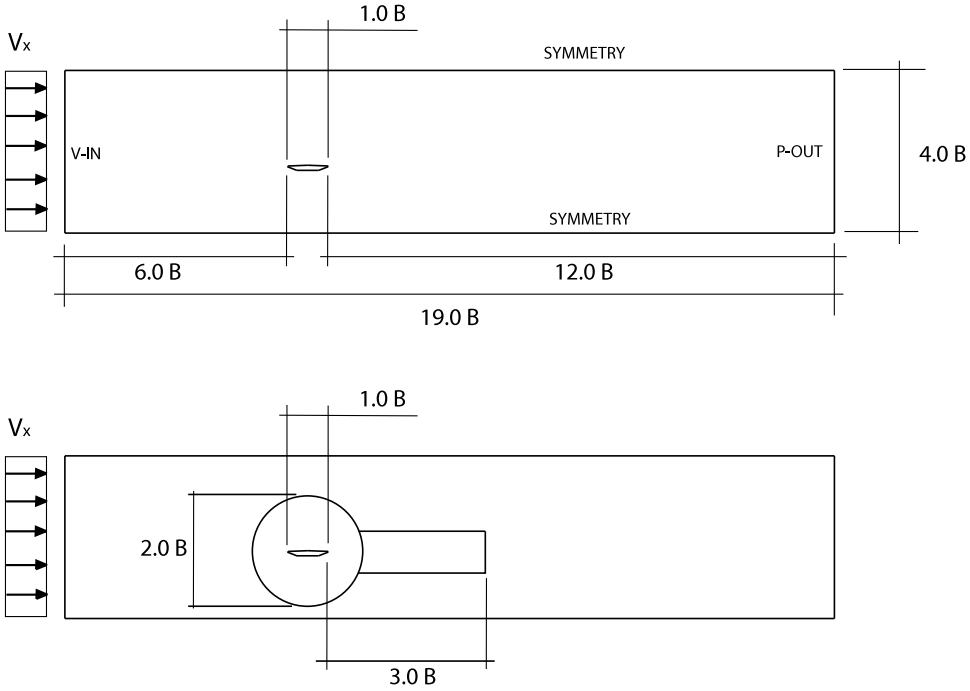

Fig. 9. Geometry and boundary conditions used in numerical simulations

In numerical simulations an ideal geometry for the deck section is used, neglecting superficial roughness and corner shape imperfections.

Mesh and Settings

The computational grid was defined through refining tests to obtain a mesh-independent solution. To lower the computational effort, a wall function is used to model flow in the near-wall region, reducing the number of elements required in the boundary layer with respect to the wall-treatment approach. A structured grid is used in the boundary layer to both achieve the fine resolution of the flow structure in this region and obtain a regular mesh around the corners of the deck profile, as shown in Fig. 10.

Triangular elements with nonstructured mesh are used for the remaining region of the fluid domain. A total of 58,936 elements are used to construct the overall computational grid. A circular region around the deck section is set to manage the different angles of attack without modifying the refined mesh near the surfaces. Besides, a dense mesh region downwind the trailing edge is provided to correctly simulate the turbulent wake effects (Fig. 11). Because the global aerodynamics of the deck are influenced by the flow separation occurring on the upwind surfaces, the mesh and choice of the turbulence model are critical for the numerical solution.

Turbulence Modeling

Turbulence modeling is a critical matter in bluff body aerodynamics, when separated flow fields are present. Different turbulence models were tested: k-ε standard (STD), k-ε Murakami-Mochida-Kondo (MMK), k-ω shear stress transport (SST), and Reynolds stress model (RSM).

A standard k-ε model is used just for comparison reasons to better assess the improvement of more sophisticated approaches. Its limitations in the description of complex flows with separation and a strong stream line curvature and its tendency to overestimate the turbulence production in the impingement region, whose convection around the body results in a reduction of the extent of the flow separation, are known.

A k-ε MMK model, widely adopted in building aerodynamics, is used to overcome the k-ε STD limitation in predicting flow separation around sharp edges. This model is not implemented in *FLUENT 6.3*, but it has been added by customized user-defined functions (UDFs), introducing a new expression for the turbulence kinetic energy production term (Tsuchiya et al. 1997).

Results obtained with these simple k-ε models are compared with those obtained with the k-ω SST and RSM. The first is suitable for complex boundary layer flows under an adverse pressure gradient, even if separations are early and overpredicted, whereas the second one takes into account the anisotropies arising because of the flow separation around the edges. Every model is used in conjunction with standard wall functions for the near-wall flow field.

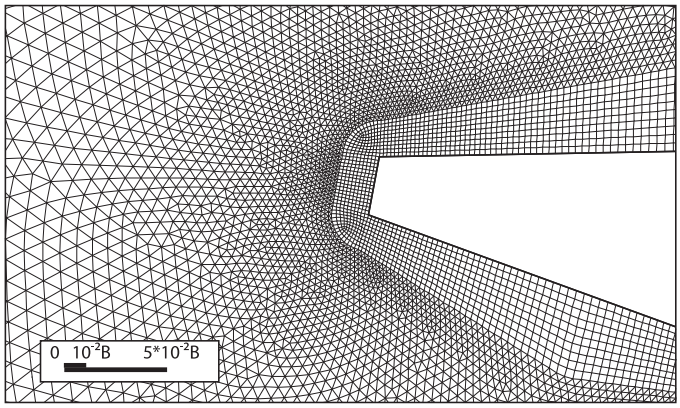

Fig. 10. Boundary layer achieved by means of a structured mesh around the deck section

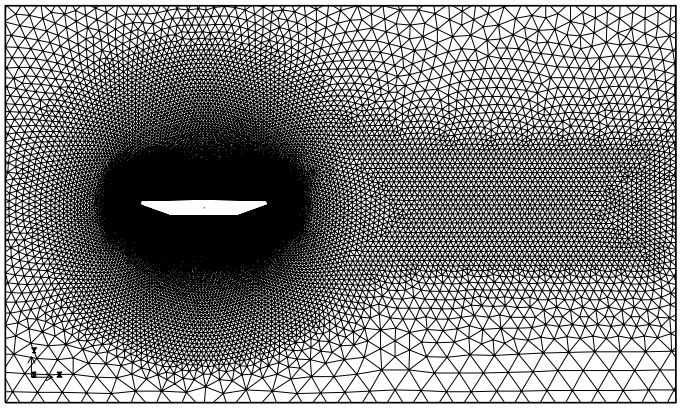

Fig. 11. Dense region behind the trailing edge

CFD Results

Two parameters, δ and ε, are defined on the basis of the analysis of the experimental pressure results previously presented (Fig. 12). The parameter δ is the distance between the leading edge and the point along the upwind lower surface where the pressure value changes its sign, whereas ε represents the reattachment length on the upper surface, measured from the leading edge. These points are defined only if they are existent.

Figs. 13 and 14 show the trend of these parameters as a function of the angle of attack, estimated both experimentally and numerically. An offset of approximately 2° between the experimental and numerical curves could be estimated, relying on δ, which is more reliable than ε for high positive angles. Extensive investigations about this offset were performed varying the simulation parameters (domain extension, boundary conditions, sharp-rounded edges). Because this effect cannot be explained from a numerical point of view, it could be related to an experimental issue.

In the following, the numerical results will be compared taking into account this offset. As an example, Fig. 15 shows how this offset leads to a good agreement between the numerical and experimental results in terms of pressure distributions for different angles of attack.

Considering the experimental results at 0° compared with the numerical one at 2° (Fig. 16), a similar pressure distribution is predicted on the lower surface by all the turbulence models, whereas higher discrepancies appear on the upwind upper surface. The k-ω SST underestimates the regions with negative pressures in the lower surface compared with the other models, whereas, in the upper upwind part close to the separation corner, it shows the best result.

Fig. 17 shows how the different models simulate the separation around the leading edge. This region is very important for the lift and moment coefficients. Looking at the slopes of the pressure distribution just around the corner and close to the reattachment point, it is possible to appreciate the different results.

- The k-ε STD predicts a strong negative initial slope, with an overestimation of the very first pressure values, producing a completely wrong separation bubble with a small ε.
- The RSM has a slightly negative initial slope that leads to an underestimation of the negative pressure values, but it accurately predicts the pressure distribution in the reattachment region.

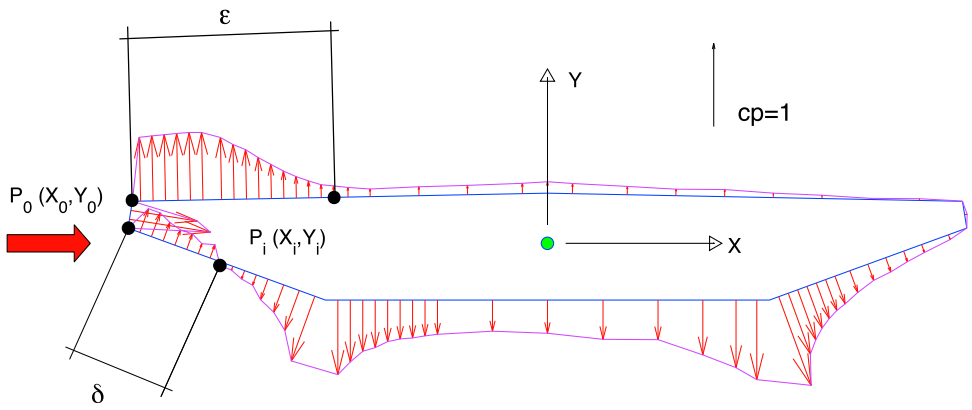

Fig. 12. Parameters δ and ε for the identify angle of attack discrepancy between experimental and numerical results

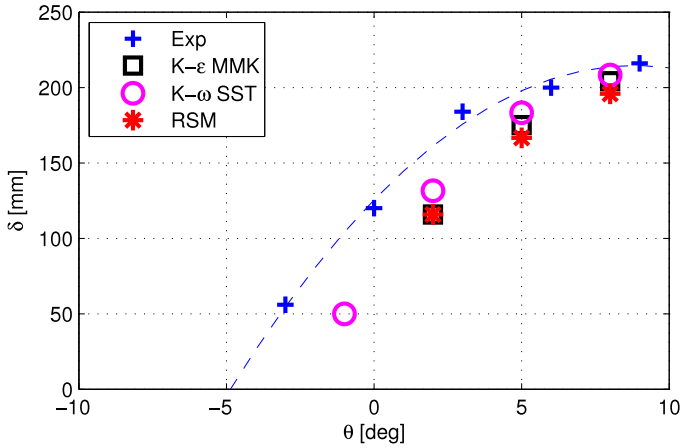

Fig. 13. Parameter δ trend versus angle of attack

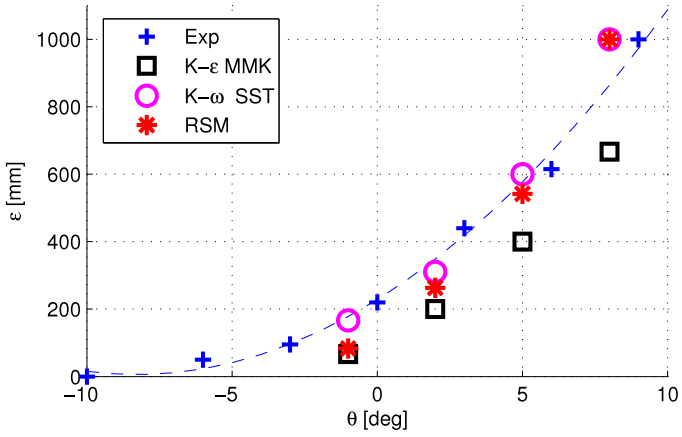

Fig. 14. Parameter ε trend versus angle of attack

- The k-ε MMK underestimates the separation bubble, even if it presents a small initial slope, close to the experimental one, and a comparable value for ε.
- The k-ω SST produces the best results in the initial part, showing pressure values and a slope close to the experimental ones, but it overestimates the ε value.

Similar considerations hold for the other angles of attack (Fig. 15). At negative angles of attack, the numerical pressure field fits the experimental measurement both in the lower and upper surfaces. In particular, the k-ω SST model is closer to the experimental results in the lower region than the RSM model, whereas in the upper region (positive pressure), both models reproduce the same behavior in a satisfactory way.

At positive angles of attack, only the upper region is critical for numerical simulation. Similar pressure distribution is obtained by both turbulence models, but the RSM model seems to better fit the reattachment length.

At strongly positive angles of attack, k-ω SST correctly reproduces the shape of the pressure distribution only in the upwind region, introducing error in the upper downwind part. A possible explanation of this behavior could be the wall-function approach. In fact, a low magnitude reverse flow is present in this section and a wall function could amplify the flow to enforce the boundary layer function. The RSM model gives a uniform underestimated pressure field in all the upper surfaces.

Comparison between Pressure Integration and Dynamometric Balance

Numerical results are used to assess the effects of shear stresses and the integration error caused by the discretized pressure measurement grid on the aerodynamic force coefficients. This analysis, in conjunction with the analysis of the experimental axial correlation of the pressure field, gives a useful tool to identify the causes of the differences between the two measurement systems.

Focusing on the drag coefficient, which has more relevant differences, it is therefore possible to identify a correction of the experimental pressure integration, consisting of three distinct terms: correlation error, discretization error, and τ error.

The correlation error for each line (A, B, C, and D) is computed from the experimental data as the ratio between the mean of the pressure values along the correlation line and the one of the correspondent central tap. The pressure magnitude measured by the taps nearby (± 0.1 m) each correlation line is scaled with these correction factors.

The discretization error is computed integrating the CFD results, sampling the pressure field with a different spatial resolution. In particular, the error is defined comparing a grid equivalent to the experimental one (78 equivalent taps) and the finer CFD grid (522 equivalent taps).

To estimate the contribution of the shear stresses in the definition of the global force, a percentage error is computed in the numerical

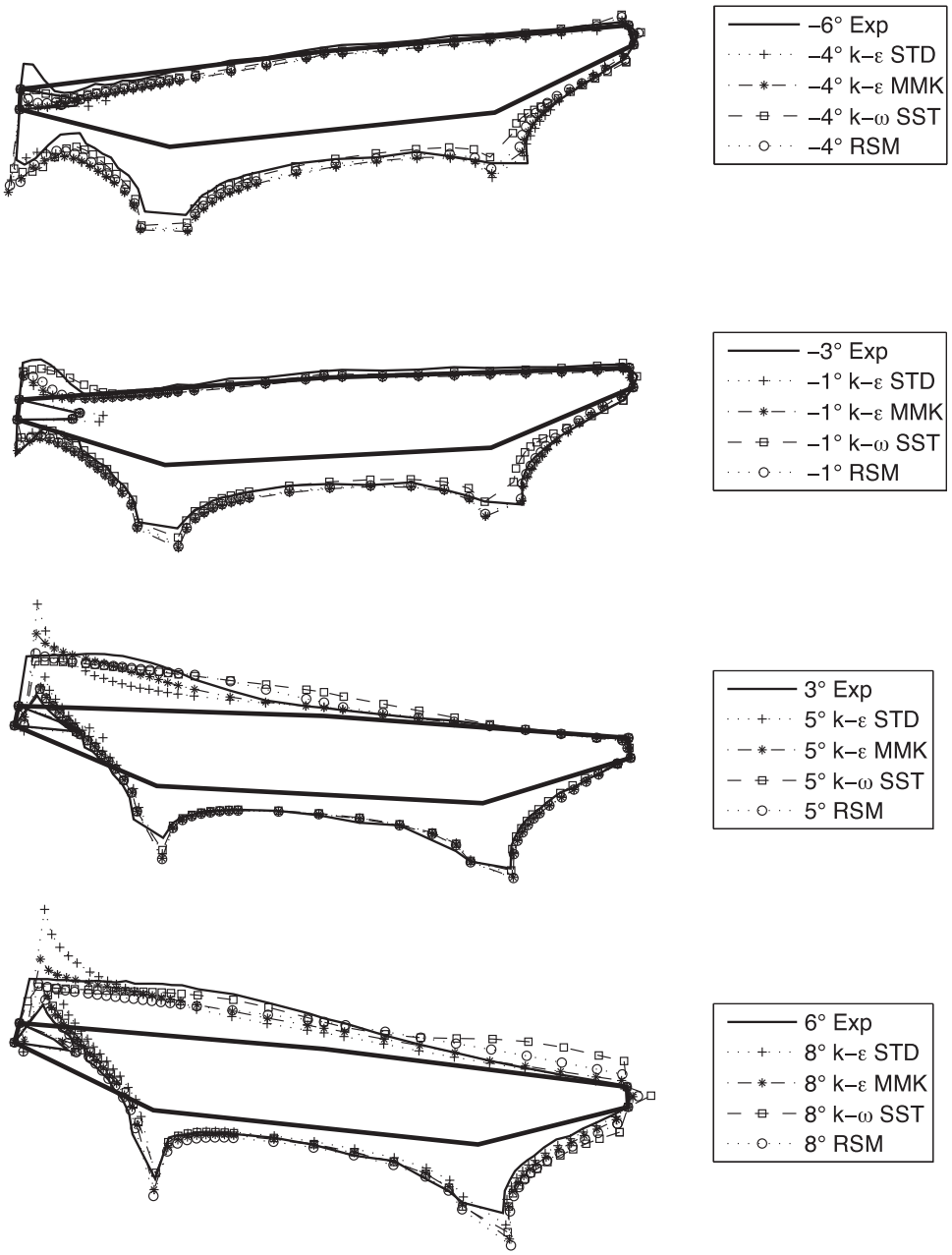

Fig. 15. Pressure distribution around the deck section at different angles of attack

analysis comparing the aerodynamic coefficients obtained integrating both normal and shear stresses with those obtained integrating only normal stresses. These errors have been evaluated for the k-ε MMK, k-ω SST, and RSM turbulence models, and similar results are obtained. Fig. 18 shows the estimated error on the drag coefficient measured with pressure integration for different angles of attack using the k-ω SST CFD results. The solid line represents the total error that is the sum of the correlation error (black bar), discretization error (gray bar), and shear-stress error (white bar).

Looking at the trends of the three errors, the following points can be observed.

1. The effect of the axial correlation of the pressure field is relevant for negative angles of attack. This effect is mainly caused by the A and B correlation lines. As shown in Fig. 6, the lower downwind surface (A correlation line) gives a positive contribution to the drag global force, whereas the lower upwind surface (B correlation line) gives a negative one. Therefore, referring to Fig. 8, the underestimation of the A pressure modulus together with the overestimation of the B one lead to an underestimation of the global drag force.
2. The discretization of the pressure field leads to an overestimation of the global drag coefficient caused by the rough description of pressure gradients, particularly on the leading edge frontal surface. For this reason the maximum error is done at $\theta = 0°$ where the contribution of this surface to the global drag force is maximum.
3. The shear-stress effect is not negligible for an accurate estimate of the global drag coefficient. Neglecting this effect leads to an underestimation of the drag coefficient with a parabolic trend with a maximum of -15% around $\theta = 0°$.

Negligible effects of τ, discretization, and the correlation of C_L and C_M are encountered ($<1\%$).

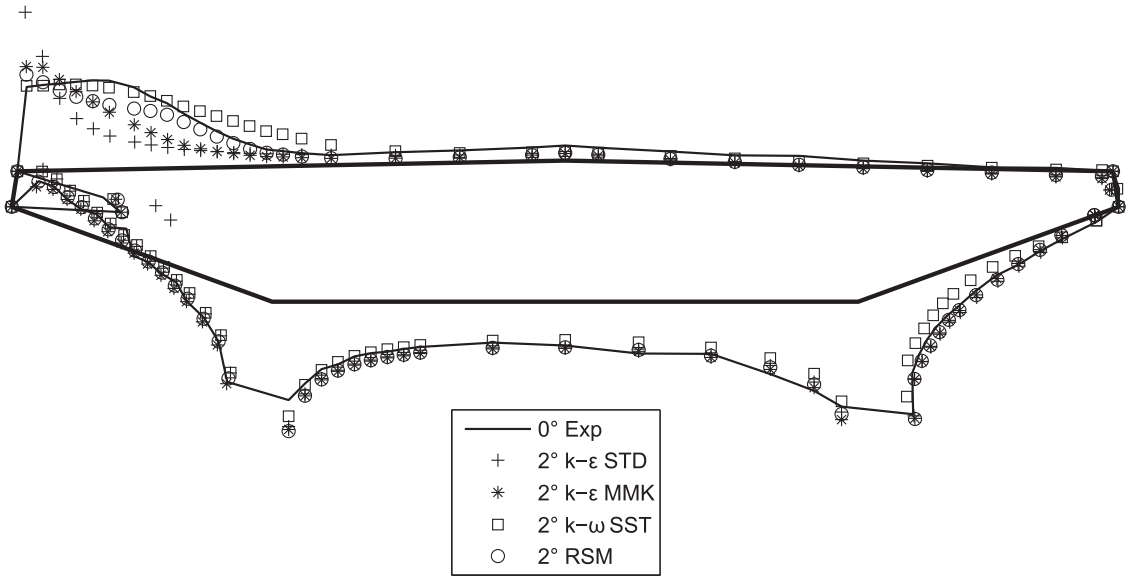

Fig. 16. Pressure distribution around the deck section at 0°

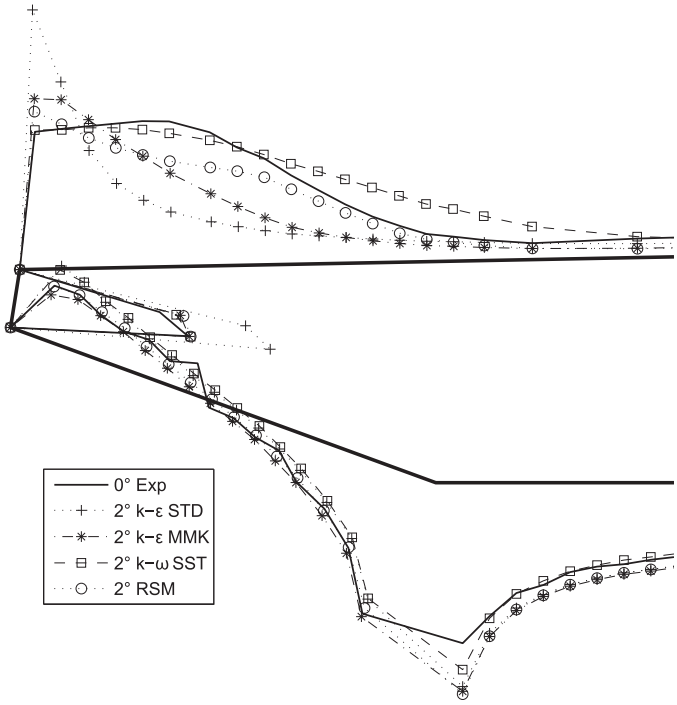

Fig. 17. Zoom of pressure distribution around the deck section at 0°

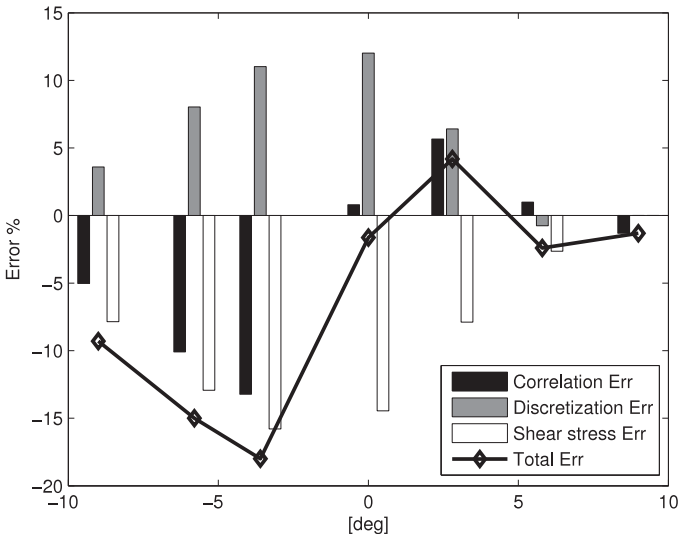

Fig. 18. Error contributions for the drag coefficient

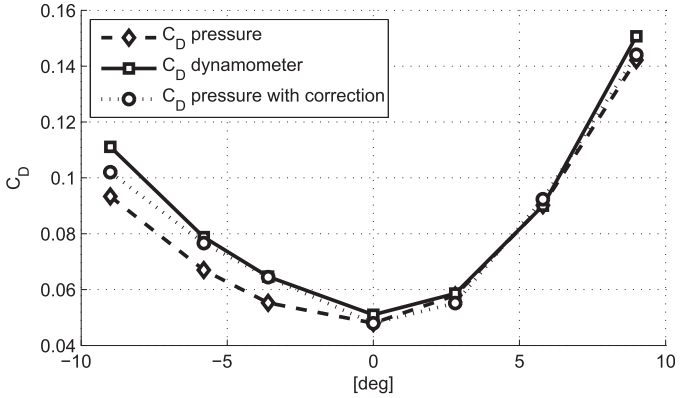

Fig. 19. Comparison of the drag coefficient curves: pressure, dynamometer, and corrected pressure

Fig. 19 shows the comparison between the drag coefficient curve measured by the dynamometric balance and the one obtained by the integration of the measured pressure field. The pressure-integrated curve is plotted, applying the correction for the estimated error (Fig. 18), and the result shows a good match with the dynamometric measurements.

Concluding Remarks

In this paper the authors presented an extended comparison between two different measurement systems for the global aerodynamic forces on a bridge deck: a dynamometric balance and a pressure field

integration. The pressure measurement has the advantage of showing the distribution of the aerodynamic force field; however, it has some intrinsic critical issues that have been pointed out and deeply studied.

The following three main effects should be accounted for: axial correlation, discretization of the pressure measurement grid, and shear-stress contribution. A 2D CFD analysis together with the experimental results allowed for evaluation of the absolute and relative weight of these three effects on the global force coefficients, pointing out that the drag force coefficient is the most sensitive. By correcting the pressure integrated coefficients a good matching of the two measurement system's results is achieved.

The correlation error could be reduced using multiple integration path lines along the deck axis to take into account the 3D flow field and achieve a more robust global averaging. The discretization error shows that a fine measurement grid must be adopted for such deck shapes to better describe the pressure gradients on the frontal surfaces that are the main responsible for the drag force generated by normal stresses. The CFD results may help in minimizing the discretization error in the design stage of the wind tunnel tests. The viscous stress effect could be estimated with CFD simulations; nevertheless, in a real bridge deck shape with barriers and railings, its contribution is less important.

References

Argentini, T., Rocchi, D., Muggiasca, S., and Zasso, A. (2012). "Cross-sectional distributions versus integrated coefficients of flutter derivatives and aerodynamic admittances identified with surface pressure measurement." *J. Wind Eng. Ind. Aerodyn.*, 104–105(May–Jul), 152–158.

Bai, Y., Sun, D., and Lin, J. (2010). "Three dimensional numerical simulations of long-span bridge aerodynamics, using block-iterative coupling and DES." *Comput. Fluids*, 39(9), 1549–1561.

Diana, G., Resta, F., and Rocchi, D. (2008). "A new numerical approach to reproduce bridge aerodynamic non-linearities in time domain." *J. Wind Eng. Ind. Aerodyn.*, 96(10–11), 1871–1884.

Diana, G., Resta, F., Zasso, A., Belloli, M., and Rocchi, D. (2004). "Forced motion and free motion aeroelastic tests on a new concept dynamometric section model of the Messina suspension bridge." *J. Wind Eng. Ind. Aerodyn.*, 92(6), 441–462.

Diana, G., Rocchi, D., and Argentini, T. (2013). "An experimental validation of a band superposition model of the aerodynamic forces acting on multi-box deck sections." *J. Wind Eng. Ind. Aerodyn.*, 113(Feb), 40–58.

Diana, G., Rocchi, D., Argentini, T., and Muggiasca, S. (2010). "Aerodynamic instability of a bridge deck section model: Linear and nonlinear approach to force modeling." *J. Wind Eng. Ind. Aerodyn.*, 98(6–7), 363–374.

FLUENT 6.3 [Computer software]. Canonsburg, PA, Ansys.

Hui, M. C. H., Zhou, Z. Y., Chen, A. R., and Xiang, H. F. (2008). "The effect of Reynolds numbers on the steady state aerodynamic force coefficients of the Stonecutters Bridge deck section." *Wind Struct.*, 11(3), 179–192.

Mannini, C., Šoda, A., Voss, R., and Schewe, G. (2010). "Unsteady RANS simulations of flow around a bridge section." *J. Wind Eng. Ind. Aerodyn.*, 98(12), 742–753.

Ricciardelli, F., and Hangan, H. (2001). "Pressure distribution and aerodynamic forces on stationary box bridge sections." *Wind Struct.*, 4(5), 399–412.

Sarwar, M., Ishihara, T., Shimada, K., Yamasaki, Y., and Ikeda, T. (2008). "Prediction of aerodynamic characteristics of a box girder bridge section using the LES turbulence model." *J. Wind Eng. Ind. Aerodyn.*, 96(10–11), 1895–1911.

Tsuchiya, M., Murakami, S., Mochida, A., Kondo, K., and Ishida, Y. (1997). "Development of a new $k-\varepsilon$ model for flow and pressure fields around bluff body." *J. Wind Eng. Ind. Aerodyn.*, 67–68(Apr), 169–182.

Watanabe, S., and Fumoto, K. (2008). "Aerodynamic study of slotted box girder using computational fluid dynamics." *J. Wind Eng. Ind. Aerodyn.*, 96(10–11), 1885–1894.

Watanabe, S., Inoue, H., and Fumoto, K. (2004). "An estimation of static aerodynamic forces of box girders using computational fluid dynamics." *Wind Struct.*, 7(1), 29–40.